Stratification of Heterogeneity in the Lithosphere of Mars From Envelope Modeling of Event S1222a and Near Impacts: Interpretation and Implications for Very-High-Frequency Events

S. Menina, L. Margerin, T. Kawamura, G. Heller, M. Drilleau, Z. Xu, M. Calvet, R. F. Garcia, B. Knapmeyer-Endrun, S. Carrasco, et al.

AGU ADVANCING EARTH AND SPACE SCIENCE

Geophysical Research Letters®

RESEARCH LETTER
10.1029/2023GL103202

Special Section:
The Large Marsquake of Sol 1222

Stratification of Heterogeneity in the Lithosphere of Mars From Envelope Modeling of Event S1222a and Near Impacts: Interpretation and Implications for Very-High-Frequency Events

S. Menina[1], L. Margerin[2], T. Kawamura[1], G. Heller[3], M. Drilleau[4], Z. Xu[1], M. Calvet[2], R. F. Garcia[2,4], B. Knapmeyer-Endrun[5], S. Carrasco[5], K. Onodera[6], P. Lognonné[1], A. Stott[4], and W. B. Banerdt[7]

[1]Université Paris Cité, Institut de Physique du Globe de Paris, CNRS, Paris, France, [2]Institut de Recherche en Astrophysique et Planétologie, Université Toulouse 3 Paul Sabatier, CNRS, Toulouse, France, [3]CEA, DAM, DIF, Arpajon, France, [4]Institut Supérieur de l'Aéronautique et de l'Espace SUPAERO, Toulouse, France, [5]Bensberg Observatory, University of Cologne, Bergisch Gladbach, Germany, [6]Earthquake Research Institute, The University of Tokyo, Tokyo, Japan, [7]Jet Propulsion Laboratory, California Institute of Technology, Pasadena, CA, USA

Abstract We have modeled the high-frequency seismogram envelopes of the large event S1222a and four recently identified near impacts recorded by the InSight mission by introducing a stratification of velocity and attenuation into a multiple-scattering approach. We show that a simple conceptual model composed of a strongly diffusive, weakly attenuating layer overlying a transparent medium captures the essential features of the observed envelopes. The attenuation profiles reveal that the minimal extension of heterogeneities at depth is of the order of 20 km in the vicinity of InSight and 60 km on the path to S1222a. We interpret this result as an indication that the Martian crust as a whole is at the origin of the strong scattering. Our heterogeneity model suggests that the sources of a number of distant Very-high-Frequency seismic events are shallow and located to the south or in close vicinity of the Martian dichotomy.

Plain Language Summary The seismometers deployed at the surface of Mars in the framework of the Interior Exploration using Seismic Investigations, Geodesy and Heat Transport mission have recently recorded seismic waves generated by meteorite impacts and a very large Marsquake. These exceptional data offer the opportunity to study how seismic waves propagate in the interior of Mars and more particularly how they attenuate. This is an important topic because attenuation characterizes the physical state of planetary interiors. There are two basic mechanisms at the origin of seismic attenuation: "absorption," which is highly sensitive to the presence of fluids—such as water—in the porosity of the rocks and "scattering," which is caused by the geological heterogeneity at length scales ranging from tens of meters to kilometers. Using advanced modeling techniques which allow for the separate quantification of the two processes, we have determined that scattering is the dominant seismic attenuation mechanism on Mars, that originates from a heterogeneous and dry crust. In the light of this result, we have revised previous interpretations of specific seismic events with a predominantly high-frequency content and propose that they originate from the vicinity of a major geological feature known as the Martian dichotomy.

Key Points:

- Envelope modeling of event S1222a and near impacts reveals a strong stratification of scattering properties in the lithosphere of Mars
- The whole crust acts as a diffusive layer with a minimal thickness of 20 km below InSight and 60 km at the location of S1222a
- Distant Very-high-Frequency events are shallow quakes or impacts originating from the south or the vicinity of the Martian dichotomy

Supporting Information:

Supporting Information may be found in the online version of this article.

Correspondence to:

S. Menina,
menina@ipgp.fr

Citation:

Menina, S., Margerin, L., Kawamura, T., Heller, G., Drilleau, M., Xu, Z., et al. (2023). Stratification of heterogeneity in the lithosphere of Mars from envelope modeling of event S1222a and near impacts: Interpretation and implications for Very-high-Frequency events. *Geophysical Research Letters*, *50*, e2023GL103202. https://doi.org/10.1029/2023GL103202

Received 9 FEB 2023
Accepted 28 MAR 2023

1. Introduction

Seismic attenuation is a key process characterizing the state of planetary interiors. When the first seismic data collected in the framework of the Apollo missions were analyzed, it was promptly realized by seismologists that the long duration of lunar seismograms was indicative of a very low level of elastic energy dissipation in the lunar lithosphere as compared to the Earth (Latham et al., 1969). The inferred very high intrinsic shear quality factor $Q_\mu \approx 3{,}500$ has later been attributed to the generally dry conditions on the Moon and more specifically to the absence of volatiles in the porosity of the lunar crust (Tittman, 1977; Tittmann et al., 1980). Absorption of energy through inelastic processes is one essential component of seismic attenuation. The other key mechanism is scattering which finds its origin in the presence of small-scale heterogeneities in the lithosphere (Aki, 1969; Dainty et al., 1974). The development of the coda following ballistic arrivals is a prominent manifestation of the central role played by scattering in shaping high-frequency seismograms (>1 Hz). In planetology, the scattering

strength is most often quantified with the aid of a diffusivity (denoted D and expressed in km^2/s) which measures the efficacy of seismic energy transport through a heterogeneous medium. The diffusivity is related to the attenuation length l of ballistic waves by the formula (Sato et al., 2012):

$$D = \frac{cl}{3}, \tag{1}$$

where c is the speed of propagation of the waves and the factor 3 in the denominator is related to the 3-dimensional character of the propagation. Because they dominate the scattered wavefield (Aki, 1992), we can consider that all quantities in Equation 1 refer to shear waves.

Early determinations of the diffusivity of the lunar crust suggested extremely low values of the order of 2 km^2/s (Latham et al., 1969), thought to be representative of a highly fractured medium. This value is to be contrasted with the one typically found in the continental crust of the Earth at the same frequency. Sato (2019a) has conducted a comprehensive compilation of estimates of scattering attenuation from the literature. With the exception of volcanoes, where diffusivities as low as 0.1 km^2/s have been reported (e.g., Wegler, 2004), the typical value $D \approx 100$ km^2/s in the continental crust of the Earth is about two orders of magnitude larger than on the Moon. Because scattering attenuation is highly sensitive to the geology, this parameter is therefore particularly interesting to quantitatively compare the seismic environment across planets.

Following the deployment of Seismic Experiment for Interior Structure (SEIS) on the surface of Mars in the framework of the InSight mission (Lognonné et al., 2019), a number of Very-high-Frequency (VF) seismic events with a good signal-to-noise ratio (SNR) in the 2–10 Hz frequency band were detected by the Marsquake Service (Ceylan et al., 2022). The data show two emergent arrivals with a rise time of a few tens of seconds, followed by a long-lasting coda (see Figure 1a). Polarization analysis has revealed a complete lack of coherency between the horizontal components of the ground motion (Carrasco et al., 2022; Lognonné et al., 2020). These observations indicate that VF signals originate from the propagation of elastic waves in a multiple-scattering environment (see van Driel et al. (2021), Karakostas et al. (2021), and Menina et al. (2021), for further arguments). These events are therefore ideal candidates to study the distribution of scattering properties in the interior of Mars with two important shortcomings: the lack of determination of the back azimuth and the absence of data at epicentral distances smaller than about 500 km.

Fortunately, the Marsquake catalog has recently been enriched with particularly interesting events. In the distance range 50–250 km, four impacts have been recorded by SEIS and their precise locations, first determined seismically, have been further refined by orbital imaging (Garcia et al., 2022). In addition, with a magnitude $M_w = 4.7$, the largest seismic event ever recorded (S1222a) has been located in the vicinity of the Martian dichotomy at an epicentral distance of $37 \pm 1.6°$ from InSight (Kawamura et al., 2022). At high frequencies, this event is strikingly similar to VF events, but also shows clear excitation of surface waves at low frequencies, a strong argument in favor of a shallow source. As a consequence of the large difference in back azimuth estimates from body and surface waves (of the order of ≈25°), S1222a may have occurred either slightly to the north or up to ≈300 km to the south of the dichotomy (Panning et al., 2022). The joint analysis of near impacts, VF events and S1222a offers the opportunity to constrain the scattering attenuation profile in the lithosphere of Mars and constitutes the main topic of this article.

2. Depth Extent of Heterogeneity From Seismogram Envelope Modeling

2.1. Evidence for the Stratification of Scattering Properties

Menina et al. (2021) used elastic radiative transfer theory in a uniform half-space to model the high-frequency envelopes of VF seismograms. They reported an overall good agreement between the predictions of the multiple-scattering model and the data and inferred the path average attenuation properties between each VF event and the InSight landing site. They found that both the diffusivity and intrinsic shear quality factor increase rapidly with epicentral distance. Because the depth of the ray turning point also increases with distance, these authors proposed that the trend inferred from the data could reflect a decrease of attenuation with depth rather than a genuine lateral variation of attenuation around InSight. Following the multiple-scattering approach of Menina et al. (2021), we introduce in the present work a stratification of velocity and attenuation as shown in Figure 1c. In a first approximation, we consider simple conceptual models composed of a single strongly

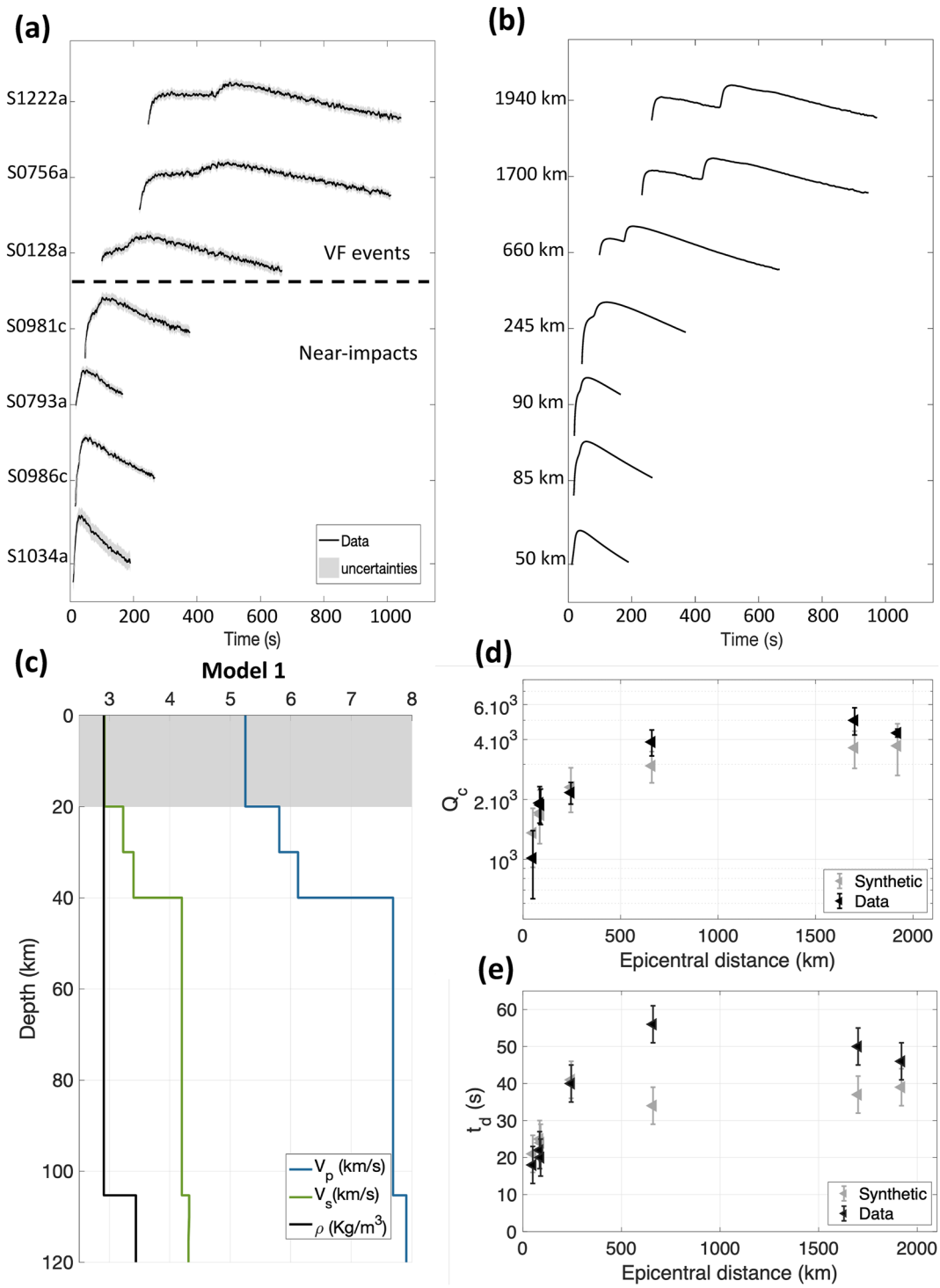

Figure 1. Comparison between *smoothed* synthetic and observed seismogram envelopes in a simple stratified model of the lithosphere (*window duration of* 5*s*). (a) Composite plot showing observed envelopes of near impacts and Very-high-Frequency (VF) events at a central frequency of 7.5 Hz. The epicentral distance increases from bottom to top. Time is measured from the occurrence of each event. (b) Composite plot showing synthetic envelopes calculated in the model shown in panel (c) at a series of epicentral distances (as indicated on the left axis) corresponding to impacts and VF events. To represent the envelopes, the same logarithmic scale is used on the vertical axes in panel (a and b). (c) Typical velocity and density profile used to model near impacts. The shaded area delimits a layer of strong scattering. (d, e): Comparison between observed and modeled delay time (t_d) and coda quality factor (Q_c) for the events shown in panel (a). *Uncertainties on* t_d and Q_c *are estimated from the smoothing window duration and the standard deviation of robust linear least squares, respectively*.

scattering layer overlying a transparent medium. A key point of our study is to demonstrate that SEIS data allow to constrain the minimal thickness of such a layer.

Let us first illustrate how a simple two-layer model captures remarkably well the overall features of near impacts and VF events envelopes including S1222a. The method developed to adjust the parameters of the model will be explained in Section 2.2. Full details on the models are provided in Tables S1–S28 in Supporting Information S1. In Figure 1b, we plot a series of energy envelopes calculated in the model shown in Figure 1c with $D \approx 10$ km^2/s, $Q_\mu \approx 3{,}000$, at epicentral distances corresponding to the impacts and event data shown in Figure 1a. The central frequency is 7.5 Hz, which offers the best SNR for most events. Qualitatively, the model reproduces a number of features seen in the data as epicentral distance increases: Gradual emergence of the *P* and *S* phases at short distance (<250 km), broadening of the seismogram envelope and progressive flattening of the *S*-coda decay curve at larger distance (>500 km). The clearest discrepancy between the model predictions and the data is visible on the distant VF events: while the *P*-coda appears relatively flat in Figure 1a, it shows a decay that is roughly parallel to the *S*-coda in Figure 1b. This important point will be examined in Section 2.2.2.

For a quantitative comparison between the synthetics and observations, we have measured two empirical parameters which classically characterize the shape of envelopes (Blanchette-Guertin et al., 2012): The peak delay time t_d—the time between the onset of *S*-waves and the energy maximum (Sato, 1989)—and the coda quality factor Q_c (Aki & Chouet, 1975). The results are shown in Figures 1d and 1e, respectively. We observe in both data and model predictions that t_d increases up to an epicentral distance of 250 km and stabilizes beyond that point. As pointed out by Gillet et al. (2017), such a feature is characteristic of a stratification of heterogeneity. The rapid increase of the coda quality factor with distance is also well reproduced by the simple two-layer model, thereby confirming its relevance to the interpretation of SEIS data. The important message from Figure 1 is that the dependence of envelope shapes on epicentral distance can in a first approximation be explained by a stratification of attenuation, without invoking ad hoc large lateral variations of propagation properties as found in Menina et al. (2021).

2.2. Thickness of the Scattering Layer

To determine the depth extent of the scattering layer, we assume a priori values for the thickness of the top-layer $h \in \{10, 15, 20, \cdots\}$ km. For each h, we perform a linearized iterative optimization of the diffusivity and shear quality factor in the layer by minimizing the misfit between the observed and synthetic energy envelopes denoted $E_{o,m}(r, t)$, respectively, with r the epicentral distance and t the time measured from the signal onset. To reduce the fluctuations, a moving average is applied to the envelopes with a 5s long time-window. For the misfit function, we select:

$$\chi^2 = \int_0^T \left(\log_{10}(E_o(r,t)/E_o^n) - \log_{10}(E_m(r,t)/E_m^n)\right)^2 dt, \tag{2}$$

where T is the signal duration as determined by SNR ≥ 2. Following the coda normalization principle (Rautian & Khalturin, 1978; Tsujiura, 1978), we remove the unknown source term from the data by normalizing both the synthetic and observed envelopes by energy integrals $E_{m,o}^n$ computed in a late time window $[T - t^n, T]$ at the end of the coda ($t^n \approx 30$ s). Because we seek to reproduce the overall shape of the envelopes, we introduce the logarithm of the energy in the definition of χ^2 to give approximately equal weights to the coda and the main arrivals. This point is particularly important for the separation of attenuation mechanisms. In the model, we assume that the bulk quality factor Q_κ is infinite, hence the relation $Q_p/Q_s = 3/4(c_p/c_s)^2$ between the *P* and *S* absorption quality factors (with $c_{p,s}$ the *P*, *S* wavespeeds). As suggested by observations of various geological objects on a broad range of scales, a correlation function of Von Kármán type is assumed. It is essentially specified by two parameters: the Hurst exponent κ and the correlation length l_c (Sato, 2019b; Wu et al., 1994). We explore two classes of media with $\kappa = 1/2$ (also known as exponential) and $\kappa = 2$ and test different values of l_c in the range [25,250] m. For each model of heterogeneity, we optimize the scattering and absorption mean free time in the top layer by minimizing χ^2 and deduce in turn the value of D and Q_μ. For source modeling, we consider instantaneous and isotropic injection of energy at a point with an *S*-to-*P* energy partitioning ratio $2(c_p/c_s)^3$ for impacts (vertical force radiation) and $\frac{3}{2}(c_p/c_s)^5$ for quakes (double couple radiation).

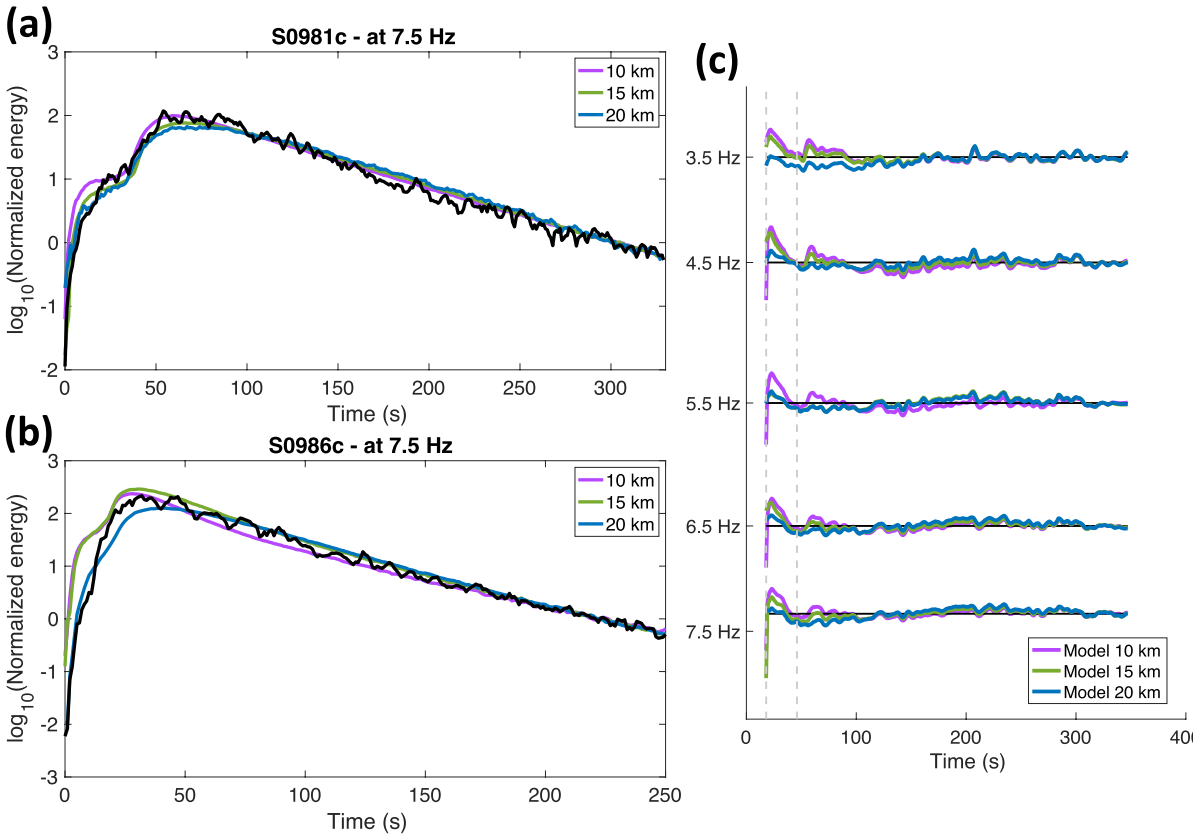

Figure 2. Determination of the minimal extension of the scattering layer at depth from envelope modeling of impacts. (a) Examples of best-fitting envelopes for event S0981c observed at 7.5 Hz. Different thicknesses of the heterogeneous layer are tested, as indicated in inset. The black line shows the data envelope for impact S0981c at 7.5 Hz frequency. (b) Same as a for event S0986c. (c) Residual between data and best-fitting envelopes for event S0981c at different frequencies, as indicated on the left of the plot. The dashed lines indicate the *P* and *S*-waves onsets. Time is measured from the start of the signals.

2.2.1. Impact Data

In Figure 2, we show the effect of varying the diffusive layer thickness h on the goodness-of-fit for impacts S0986c and S0981c, located respectively at 85 and 245 km from Insight. In the case of S0986c (Figure 2b), the smallest thicknesses $h = 10$, 15 km, predict an onset of the synthetic envelope which is too abrupt compared to the data. The misfit (as quantified by χ^2) is reduced by a factor of 2 when increasing h from 10–15 to 20 km. To appreciate the role of the layer thickness in the case of S0981c (Figure 2a), we have plotted the residuals between observations and synthetics at different frequencies (Figure 2c). It is apparent that the thickness $h = 20$ km provides the best match to the data. The improvement of the fit near the main arrivals is particularly significant since they are most sensitive to the scattering properties (Mayor et al., 2014; Onodera et al., 2022; van Dinther et al., 2021). The misfit reduction is of the order of 50% when increasing h from 10 to 20 km. From this analysis, we conclude that a diffusive layer with Hurst exponent $\kappa = 0.5$, heterogeneity scale length $l_c \approx 125$ m and thickness 20 km suffices to match the observations. Note that this top layer has relatively fast shear velocities, close to 3 km/s, which contrasts with previous findings (Knapmeyer-Endrun et al., 2021). Although the determination of the crustal velocities falls completely out of the scope of the present work, we found that relatively high shear-wave speeds are necessary to match the traveltime difference between *P* and *S* arrivals for S0981c. We note that recent models obtained from surface wave observations also suggest higher crustal velocities than previously determined below InSight (Beghein et al., 2022; Kim, Banerdt, et al., 2022; Kim, Stähler, et al., 2022).

2.2.2. The Large Event S1222a

We now examine the case of the recent large event S1222a at the same frequency as the impacts (7.5 Hz). In Figure 3c, we show the inversion results in the case of a 20 km thick diffusive layer (Model 1, same as shown in Figure 1c). As previously pointed out, this model provides a poor fit to the data. In addition to the too sharp *P* and

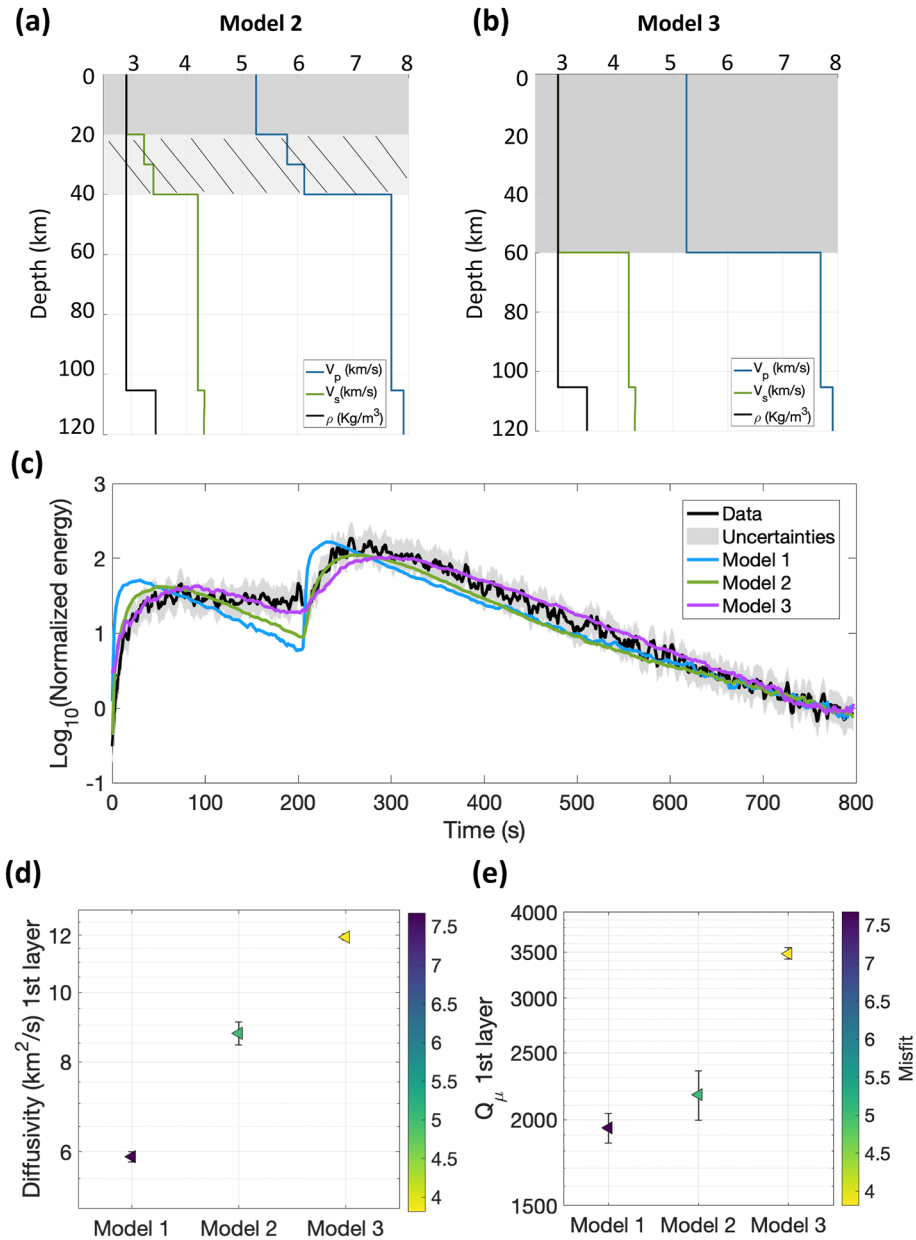

Figure 3. Determination of the minimal extension of the scattering layer at depth from envelope modeling of event S1222a. (a) Stratified scattering medium (model 2) with a 20 km thick diffusive layer at the top and an increased heterogeneity level between 20 and 40 km depth compared to model 1. (b) Two-layer medium (model 3) with a thick (60 km) diffusive layer overlying a transparent medium. (c) Best-fitting envelopes for models 1–3 (in colors, see inset) compared to the data of S1222a (black solid line). Time is measured from signal onset. (d) Best-fitting diffusivity estimate for models 1–3. (e) Best-fitting shear quality factor estimate for models 1–3. The color bars indicate the value of the misfit.

S onsets, the most obvious discrepancy is visible in the coda of *P*-waves. Whereas the model predicts a *P*-coda decay which is almost parallel to the *S*-coda, the data show a flat or slightly decreasing energy level. To explain this observation, we first explored a large variety of random media by varying κ and l_c. Because all these attempts proved unsuccessful, we then relaxed the constraint $Q_p/Q_s = \frac{3}{4}(c_p/c_s)^2$ and assumed $Q_p \gg Q_s$ to slow down the *P*-coda decay. But this approach also lead to a dead end. The reason is that the so-called *P* arrival is in fact very rapidly dominated by converted *S*-waves (Figure S1 in Supporting Information S1). A careful examination of the envelopes calculated by Menina et al. (2021) eventually provided the clue to solve our problem. Indeed, in the uniform half-space geometry, these authors found that the *P*-coda is nearly flat, as seen on S1222a as well as a

number of distant VF events such as S0756a shown in Figure 1a. To demonstrate that it is indeed the extent of heterogeneity at depth that controls the shape of the *P*-coda, we significantly increase the scattering strength in model 1 between 20 and 40 km depth. In the resulting model 2 (Figure 3a), the emergent character of the *P* and *S* arrivals is better reproduced and the decay rate of the *P*-coda is reduced. Indeed, increasing the diffusive layer thickness enhances the conversion of ballistic *P* to scattered *S* energy, which delays the arrival of the energy maximum and allows to sustain a long *P*-coda (Figure S1 in Supporting Information S1). A very satisfactory match between data and synthetics can be achieved by further increasing the thickness of the diffusive layer to 60 km (model 3). In this model (Figure 3b), the *P* and *S* onsets are generally well reproduced and the *P*-coda shows a much slower decay than the *S* coda as required. The diffusivity $D \approx 12$ km^2/s and absorption quality factor $Q_\mu \approx 3{,}500$ for the best-fitting model are remarkably close to the values deduced from impacts. The low diffusivity can be explained equally well by Von Kármán media with $\nu = 2$ and $l_c \approx 70$ m (Figure 3) or $\nu = 0.5$ and $l_c \approx 125$ m (Figure S2 in Supporting Information S1), which shows that the medium parameters are imperfectly resolved. Such trade-offs are common in envelope inversions for scattering properties (Calvet et al., 2023; Gaebler et al., 2015).

3. Interpretation and Discussion

3.1. Origin of the Scattering

From the envelope modeling of impacts and event S1222a, we find that the diffusive layer at the surface of Mars must thicken from at least $h = 20$ km in the vicinity of the InSight landing site to $h = 60$ km along the path of S1222a. We note that the latter value is in good agreement with the average crustal thickness deduced from surface wave analysis (Kim, Stähler, et al., 2022). The simplest explanation for our finding is that it is the crust as a whole which is responsible for most of the scattering and not a highly fractured 10 km-thick (or so) megaregolith. We acknowledge that there exists a trade-off between the thickness of the diffusive layer *h* and its scattering properties. This fact is apparent in Figure 3 where we observe that *D* increases with *h*. Hence, we cannot exclude that the diffusive layer is thicker than 20 km below InSight. But this would not plead in favor of the fractured megaregolith interpretation, as porosity is not expected to extend below 20 km depth (Wieczorek et al., 2022). That fractures and porosity do not extend to great depth, except in the close vicinity of InSight, is supported by the rather fast velocities required to fit the travel time of the main *P* and *S* arrivals for impacts. Furthermore, the good coincidence between the attenuation parameters deduced from the independent modeling of impacts and S1222a suggests that our estimates of the depth extent of scattering is compatible with a common crustal source of heterogeneity.

It is rather unsurprising that the differentiated crust of Mars is much more strongly scattering than the mantle. An open question is to understand why crustal materials are, on average, more strongly scattering on Mars than on Earth. Actually, a careful distinction should be made between the continental and oceanic lithosphere in the case of the Earth. It is well documented that regional propagation is vastly different between these two geological domains (Takeuchi et al., 2017). In the oceanic lithosphere, the nature of the seismic wavefield changes drastically above 2 Hz as a consequence of the widespread presence of small-scale heterogeneities (Furumura & Kennett, 2005). The emergent character and long-lasting coda of the *Po* and *So* phases at high frequency bears strong similarities with the *P* and *S* arrivals of VF events (Furumura & Kennett, 2005; Kennett et al., 2014). In both cases, the propagation mechanism at work is forward multiple scattering (Menina et al., 2021; Shito et al., 2013). Recently, Hannemann et al. (2022) have estimated a diffusivity in the range 15–60 km^2/s for the lithosphere of the Atlantic ocean, a value which does not differ much from our estimates for VF events (of the order 10 km^2/s). Based on the similarities between oceanic propagation on Earth and regional propagation on Mars, we hypothesize that it is the broadly basaltic nature of the Martian crust (e.g., Taylor & McLennan, 2009) which is at the origin of the strong scattering estimated from VF events. Note that a major difference between Earth and Mars is the very high Q_μ for the latter, which is compatible with an overall dry medium.

From an attenuation perspective, our study highlights important differences between Mars and the Moon. While their lithospheres exhibit similar levels of anelasticity, scattering is stronger by a factor of 5 and extends to greater depths (80–100 km) on the Moon than on Mars (Gillet et al., 2017). The low seismic diffusivity associated with a large porosity puts forward fractures as the dominant source of scattering on the Moon (Wieczorek et al., 2013). By contrast, our analysis of SEIS data strongly suggests that the lithology of the Martian crust is at the origin of the scattering attenuation. Of course, a mix of the two types of heterogeneities is likely but in vastly different proportions between Mars and the Moon.

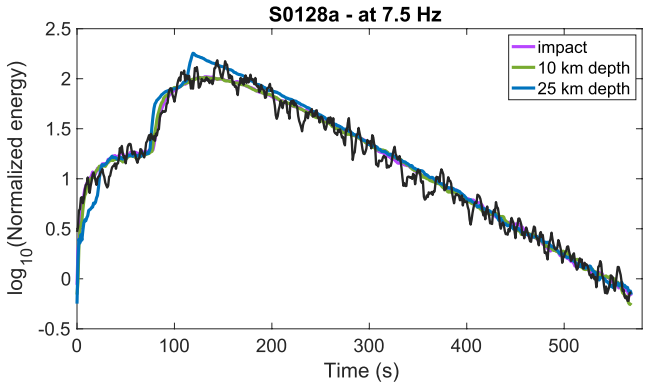

Figure 4. Constraint on the source depth of the regional Very-high-Frequency event S0128a. Three hypotheses are tested as indicated by the different colors in inset. The envelope shape of S0128a is well modeled for shallow sources. By contrast, a source located below the diffusive layer (25 km depth) produces arrivals with sharp onsets that are not seen in the actual seismogram envelopes. Time is measured from signal onset.

3.2. Implications for the Interpretation of VF Events

Our simple conceptual model for the propagation of VF events has important implications for their interpretation. First, in contrast with previous proposals (van Driel et al., 2021), we find that a highly heterogeneous, low-velocity megaregolith of 10 km thickness cannot explain the envelope shape of VF events at a regional distance. Second, our model has strong implications for their source depth. While the envelope shape of a typical VF event such as S0128a is well reproduced by assuming an impact or shallow quake (<20 km depth) scenario, a deeper focus (e.g., 25 km depth) gives rise to sharp arrivals corresponding to refracted phases which propagate only once through the diffusive layer (see Figure 4). Such arrivals are not visible in the data. Note that in the case of the deep source, the attenuation properties of the diffusive layer are re-inverted in order to best match the observations. But we found it impossible to reproduce the overall envelope shape of S0128a without generating additional spurious arrivals. Note that because the initial energy partitioning between *P* and *S*-modes at the source is very rapidly erased by multiple-scattering, the relative amplitude of the *P* and *S* arrivals bears little information on the source mechanism (see Figure 4). Hence, the origin -quake or impact- of VF events appears difficult to determine from seismic data only. Third, we remark that a number of distant VF events share envelope characteristics that are highly similar to the one of S1222a. The case of S0756a is particularly striking (see Figure 1a). In the framework of our model, this indicates that these events originate from a thick crust, hence from the south of the dichotomy or its close vicinity.

4. Conclusion

We have shown that a strong stratification of heterogeneity in the lithosphere of Mars offers a simple conceptual model to explain the main characteristics of seismic wave propagation at regional distance. The thickness of the weakly anelastic and diffusive layer increases from a minimal average value of 20 km in the vicinity of InSight to 60 km on the path to S1222a. This finding indicates that it is the whole crust of Mars which is heterogeneous and supports a lithological origin for the strong scattering required to explain the VF events. The strong similarity between the seismogram envelope of S1222a and a number of distant VF events suggests that the latter originate from the close vicinity of the dichotomy where the crust is sufficiently thick. Finally, we show that the source of VF events must necessarily be located inside the diffusive layer, hence sufficiently shallow.

Data Availability Statement

All raw waveform data is available through the InSight Mars SEIS Data Service @ IPGP, IRIS-DMC, and NASA PDS (InSight Mars SEIS Data Service, 2019). The seismicity catalog including all the events used in this study is available from Marsquake Service (InSight Marsquake Service, 2023).

Acknowledgments
We acknowledge NASA, CNES, their partner agencies and Institutions (UKSA, SSO, DLR, JPL, IPGP-CNRS, ETHZ, IC, and MPS-MPG) and the flight operations team at JPL, SISMOC, MSDS, IRIS-DMC, and PDS for providing SEED SEIS data. This work was performed using HPC resources from the CALMIP supercomputing center (Project P190038). The French co-authors acknowledge the support of CNES and ANR (under contract MAGIS ANR-19CE31-0008-08 and ANR-18-IDEX-0001). This work was performed in part at the Jet Propulsion Laboratory, California Institute of Technology, under a contract with the National Aeronautics and Space Administration (80NM0018D0004). This is InSight contribution 286.

References

Aki, K. (1969). Analysis of the seismic coda of local earthquakes as scattered waves. *Journal of Geophysical Research*, *74*(2), 615–618. https://doi.org/10.1029/jb074i002p00615

Aki, K. (1992). Scattering conversions P to S versus S to P. *Bulletin of the Seismological Society of America*, *82*(4), 1969–1972. https://doi.org/10.1785/bssa0820041969

Aki, K., & Chouet, B. (1975). Origin of coda waves, sources and attenuation. *Journal of Geophysical Research*, *80*(23), 3322–3342. https://doi.org/10.1029/jb080i023p03322

Beghein, C., Li, J., Weidner, E., Maguire, R., Wookey, J., Lekić, V., et al. (2022). Crustal anisotropy in the Martian lowlands from surface waves. *Geophysical Research Letters*, *49*(24), e2022GL101508. https://doi.org/10.1029/2022GL101508

Blanchette-Guertin, J.-F., Johnson, C., & Lawrence, J. (2012). Investigation of scattering in lunar seismic coda. *Journal of Geophysical Research*, *117*(E6), E06003. https://doi.org/10.1029/2011je004042

Calvet, M., Margerin, L., & Hung, S.-H. (2023). Anomalous attenuation of high-frequency seismic waves in Taiwan: Observation, model and interpretation. *Journal of Geophysical Research: Solid Earth*, *128*(3), e2022JB025211. https://doi.org/10.1029/2022JB025211

Carrasco, S., Knapmeyer-Endrun, B., Margerin, L., Schmelzbach, C., Onodera, K., Pan, L., et al. (2022). Empirical h/v spectral ratios at the InSight landing site and implications for the Martian subsurface structure. *Geophysical Journal International*, *232*(2), 1293–1310. https://doi.org/10.1093/gji/ggac391

Ceylan, S., Clinton, J. F., Giardini, D., Stähler, S. C., Horleston, A., Kawamura, T., et al. (2022). The Marsquake catalogue from InSight, sols 0–1011. *Physics of the Earth and Planetary Interiors*, *333*, 106943. https://doi.org/10.1016/j.pepi.2022.106943

Dainty, A. M., Toksoz, M. N., Anderson, K. R., Pines, P. J., Nakamura, Y., & Latham, G. V. (1974). Seismic scattering and shallow structure of the Moon in Oceanus Procellarum. *The Moon*, *9*(1–2), 11–29. https://doi.org/10.1007/bf00565388

Furumura, T., & Kennett, B. (2005). Subduction zone guided waves and the heterogeneity structure of the subducted plate: Intensity anomalies in northern Japan. *Journal of Geophysical Research*, *110*(B10), B10302. https://doi.org/10.1029/2004jb003486

Gaebler, P. J., Sens-Schönfelder, C., & Korn, M. (2015). The influence of crustal scattering on translational and rotational motions in regional and teleseismic coda waves. *Geophysical Journal International*, *201*(1), 355–371. https://doi.org/10.1093/gji/ggv006

Garcia, R. F., Daubar, I. J., Beucler, É., Posiolova, L. V., Collins, G. S., Lognonné, P., et al. (2022). Newly formed craters on Mars located using seismic and acoustic wave data from InSight. *Nature Geoscience*, *15*(10), 1–7. https://doi.org/10.1038/s41561-022-01014-0

Gillet, K., Margerin, L., Calvet, M., & Monnereau, M. (2017). Scattering attenuation profile of the Moon: Implications for shallow moonquakes and the structure of the megaregolith. *Physics of the Earth and Planetary Interiors*, *262*, 28–40. https://doi.org/10.1016/j.pepi.2016.11.001

Hannemann, K., Eulenfeld, T., Krüger, F., & Dahm, T. (2022). Seismic scattering and absorption of oceanic lithospheric S waves in the Eastern North Atlantic. *Geophysical Journal International*, *229*(2), 948–961. https://doi.org/10.1093/gji/ggab493

InSight Marsquake Service. (2023). *Mars seismic catalogue, InSight mission; v13 2023-01-01*. ETHZ, IPGP, JPL, ICL, University of Bristol. https://doi.org/10.12686/a19

InSight Mars SEIS Data Service. (2019). *Seis raw data, InSight mission*. IPGP, JPL, CNES, ETHZ, ICL, MPS, ISAE-Supaero, LPG, MFSC. https://doi.org/10.18715/SEIS.INSIGHT.XB_2016

Karakostas, F., Schmerr, N., Maguire, R., Huang, Q., Kim, D., Lekic, V., et al. (2021). Scattering attenuation of the Martian interior through coda-wave analysis. *Bulletin of the Seismological Society of America*, *111*(6), 3035–3054. https://doi.org/10.1785/0120210253

Kawamura, T., Clinton, J. F., Zenhäusern, G., Ceylan, S., Horleston, A. C., Dahmen, N. L., et al. (2022). S1222a-the largest Marsquake detected by InSight. *Geophysical Research Letters*, *50*(5), e2022GL101543. https://doi.org/10.1029/2022GL101543

Kennett, B., Furumura, T., & Zhao, Y. (2014). High-frequency Po/So guided waves in the oceanic lithosphere: II—Heterogeneity and attenuation. *Geophysical Journal International*, *199*(1), 614–630. https://doi.org/10.1093/gji/ggu286

Kim, D., Banerdt, W., Ceylan, S., Giardini, D., Lekić, V., Lognonné, P., et al. (2022). Surface waves and crustal structure on Mars. *Science*, *378*(6618), 417–421. https://doi.org/10.1126/science.abq7157

Kim, D., Stähler, S., Ceylan, S., Lekic, V., Maguire, R., Zenhäusern, G., et al. (2022). Structure along the Martian dichotomy constrained by Raleigh and love waves and their overtones. *Geophysical Research Letters*, *49*, e2022GL101666. https://doi.org/10.1029/2022gl101666

Knapmeyer-Endrun, B., Panning, M. P., Bissig, F., Joshi, R., Khan, A., Kim, D., et al. (2021). Thickness and structure of the Martian crust from InSight seismic data. *Science*, *373*(6553), 438–443. https://doi.org/10.1126/science.abf8966

Latham, G., Ewing, M., Press, F., & Sutton, G. (1969). The Apollo passive seismic experiment. *Science*, *165*(3890), 241–250. https://doi.org/10.1126/science.165.3890.241

Lognonné, P., Banerdt, W., Pike, W., Giardini, D., Christensen, U., Garcia, R. F., et al. (2020). Constraints on the shallow elastic and anelastic structure of Mars from InSight seismic data. *Nature Geoscience*, *13*(3), 213–220. https://doi.org/10.1038/s41561-020-0536-y

Lognonné, P., Banerdt, W. B., Giardini, D., Pike, W., Christensen, U., Laudet, P., et al. (2019). SEIS: InSight's seismic experiment for internal structure of Mars. *Space Science Reviews*, *215*(1), 12. https://doi.org/10.1007/s11214-018-0574-6

Mayor, J., Margerin, L., & Calvet, M. (2014). Sensitivity of coda waves to spatial variations of absorption and scattering: Radiative transfer theory and 2-D examples. *Geophysical Journal International*, *197*(2), 1117–1137. https://doi.org/10.1093/gji/ggu046

Menina, S., Margerin, L., Kawamura, T., Lognonné, P., Marti, J., Drilleau, M., et al. (2021). Energy envelope and attenuation characteristics of high-frequency (HF) and very-high-frequency (VF) Martian events. *Bulletin of the Seismological Society of America*, *111*(6), 3016–3034. https://doi.org/10.1785/0120210127

Onodera, K., Kawamura, T., Tanaka, S., Ishihara, Y., & Maeda, T. (2022). Quantitative evaluation of the lunar seismic scattering and comparison between the Earth, Mars, and the moon. *Journal of Geophysical Research: Planets*, *127*(12), e2022JE007558. https://doi.org/10.1029/2022je007558

Panning, M. P., Banerdt, W. B., Beghein, C., Carrasco, S., Ceylan, S., Clinton, J. F., et al. (2022). Locating the largest event observed on Mars with multi-orbit surface waves. *Geophysical Research Letters*, *50*(1), e2022GL101270. https://doi.org/10.1029/2022GL101270

Rautian, T., & Khalturin, V. (1978). The use of the coda for determination of the earthquake source spectrum. *Bulletin of the Seismological Society of America*, *68*(4), 923–948. https://doi.org/10.1785/bssa0680040923

Sato, H. (1989). Broadening of seismogram envelopes in the randomly inhomogeneous lithosphere based on the parabolic approximation: Southeastern Honshu, Japan. *Journal of Geophysical Research*, *94*(B12), 17735–17747. https://doi.org/10.1029/jb094ib12p17735

Sato, H. (2019a). Isotropic scattering coefficient of the solid Earth. *Geophysical Journal International*, *218*(3), 2079–2088. https://doi.org/10.1093/gji/ggz266

Sato, H. (2019b). Power spectra of random heterogeneities in the solid Earth. *Solid Earth*, *10*(1), 275–292. https://doi.org/10.5194/se-10-275-2019

Sato, H., Fehler, M. C., & Maeda, T. (2012). *Seismic wave propagation and scattering in the heterogeneous Earth* (Vol. 496). Springer.

Shito, A., Suetsugu, D., Furumura, T., Sugioka, H., & Ito, A. (2013). Small-scale heterogeneities in the oceanic lithosphere inferred from guided waves. *Geophysical Research Letters*, *40*(9), 1708–1712. https://doi.org/10.1002/grl.50330

Takeuchi, N., Kawakatsu, H., Shiobara, H., Isse, T., Sugioka, H., Ito, A., & Utada, H. (2017). Determination of intrinsic attenuation in the oceanic lithosphere-asthenosphere system. *Science*, *358*(6370), 1593–1596. https://doi.org/10.1126/science.aao3508

Taylor, S. R., & McLennan, S. (2009). *Planetary crusts: Their composition, origin and evolution* (Vol. 10). Cambridge University Press.

Tittman, B. (1977). Lunar rock q in 3000-5000 range achieved in laboratory. *Philosophical Transactions of the Royal Society of London - Series A: Mathematical and Physical Sciences*, *285*(1327), 475–479.

Tittmann, B., Clark, V., Richardson, J., & Spencer, T. (1980). Possible mechanism for seismic attenuation in rocks containing small amounts of volatiles. *Journal of Geophysical Research*, *85*(B10), 5199–5208. https://doi.org/10.1029/jb085ib10p05199

Tsujiura, M. (1978). Spectral analysis of the coda waves from local earthquakes. *Bulletin of the Earthquake Research Institute*, *53*, 1–48.

van Dinther, C., Margerin, L., & Campillo, M. (2021). Implications of laterally varying scattering properties for subsurface monitoring with coda wave sensitivity kernels: Application to volcanic and fault zone setting. *Journal of Geophysical Research: Solid Earth*, *126*(12), e2021JB022554. https://doi.org/10.1029/2021JB022554

van Driel, M., Ceylan, S., Clinton, J. F., Giardini, D., Horleston, A., Margerin, L., et al. (2021). High-frequency seismic events on Mars observed by InSight. *Journal of Geophysical Research: Planets*, *126*(2), e2020JE006670. https://doi.org/10.1029/2020JE006670

Wegler, U. (2004). Diffusion of seismic waves in a thick layer: Theory and application to Vesuvius volcano. *Journal of Geophysical Research*, *109*(B18), 07303. https://doi.org/10.1029/2004jb003048

Wieczorek, M. A., Broquet, A., McLennan, S. M., Rivoldini, A., Golombek, M., Antonangeli, D., et al. (2022). InSight constraints on the global character of the Martian crust. *Journal of Geophysical Research: Planets*, *127*(5), e2022JE007298. https://doi.org/10.1029/2022je007298

Wieczorek, M. A., Neumann, G. A., Nimmo, F., Kiefer, W. S., Taylor, G. J., Melosh, H. J., et al. (2013). The crust of the Moon as seen by GRAIL. *Science*, *339*(6120), 671–675. https://doi.org/10.1126/science.1231530

Wu, R., Xu, Z., & Li, X. (1994). Heterogeneity spectrum and scale-anisotropy in the upper crust revealed by the German continental deep-drilling (KTB) holes. *Geophysical Research Letters*, *21*(10), 911–914. https://doi.org/10.1029/94gl00772